AIAA AVIATION Forum
June 15-19, 2020, VIRTUAL EVENT
AIAA AVIATION 2020 FORUM

10.2514/6.2020-2760

Sonic Boom Prediction Workshop 3: Propagation Modeling using PCBoom

Robert S. Downs[1], Sophie Kaye[2], and Juliet A. Page[3]
U.S. Department of Transportation, Cambridge, Massachusetts 02142, USA

The PCBoom suite of tools was used to model atmospheric propagation cases and the optional focus case as part of the 3rd AIAA Sonic Boom Prediction Workshop. The Focused Boom module FOBoom version 6.8b was used to complete ray tracing calculations using CFD pressure data as the source. Lossy propagation was modeled using PCBoom's interactive Burgers equation solver, PCBurg, and final results were obtained with the batch analysis tool HeadlessBurgers. Modifications to the latter tool were made to add B-weighted sound exposure level to the output. The effects of sampling rate, time-step factor, and other factors on model results were investigated. Lateral cutoff angles were refined by finely incrementing azimuth angles and examining propagation paths and ground metrics near cutoff. The optional focus case, in which the vehicle trajectory included acceleration, was also modeled using PCBoom. An interactive program (RayCau) was used to generate ray diagrams showing the caustic and the delta-tangent ray to confirm the focus condition, and to facilitate identification of the ray and signature for input to the Lossy Nonlinear Tricomi Equation (LNTE) solver. PCBurg was used to obtain the lossy signature at the delta tangent position. Finally, the LNTE module was used to compute signatures in the vicinity of the focal zone.

I. Nomenclature

ASEL	=	A-weighted sound exposure level; BSEL, CSEL similarly represent B- and C- frequency weighting
c	=	speed of sound
dP	=	difference between local pressure and ambient pressure
f_{ac}	=	characteristic acoustic frequency
L	=	vehicle length
M	=	Mach number
P	=	pressure
P_{ac},	=	characteristic acoustic pressure
$P_{\max}$	=	peak overpressure
PL	=	Stevens Mark VII perceived level of loudness
R	=	pressure cylinder radius
R_{tot}	=	caustic curvature
$\bar{t}$	=	dimensionless time variable
x	=	axial coordinate, parallel to flight path
y	=	lateral coordinate, positive out left wing
z	=	vertical coordinate
$\bar{z}$	=	distance normal to the caustic divided by diffraction boundary-layer thickness
$\overline{\alpha}$	=	dimensionless absorption coefficient
β	=	coefficient of nonlinearity
ρ	=	density
$\overline{\tau}_v$	=	dimensionless relaxation time for the v-th relaxation component

[1] General Engineer, John A. Volpe National Transportation Systems Center, V-324, Member AIAA
[2] General Engineer, John A. Volpe National Transportation Systems Center, V-324
[3] Physical Scientist, John A. Volpe National Transportation Systems Center, V-324, Associate Fellow AIAA

μ = shear viscosity
ε = distance tolerance used in Ramer-Douglas-Peucker algorithm
φ = azimuth angle
δ = diffraction boundary-layer thickness
Θ = ray elevation angle

II. Introduction

The third AIAA Sonic Boom Prediction Workshop (SBPW3) was held on 4-5 January 2020 in conjunction with the AIAA Science and Technology Forum and Exposition (SciTech 2020). The workshop was conducted in two parts, the first comprising state-of-the-art for predicting near field sonic boom signatures with computational fluid dynamics (CFD) and the second covering propagation of the near-field pressures to the ground through realistic atmospheric conditions. The propagation portion of the workshop included 12 submissions representing participants from the US, Europe, and Japan. Each submitting group used their respective modeling tools and associated best practices for computing solutions for the provided cases. One goal of this workshop was to create an open forum for discussion of results and to exchange best practices. Following the success of the first two sonic boom prediction workshops held in 2008 [1] and 2017 [2], CFD and propagation test cases for the third workshop included signatures quieter than those from the second workshop in order to evaluate the effectiveness of different methods when applied to shaped sonic booms. This paper describes results submitted by the US DOT Volpe Center for the propagation cases, including the optional focusing case. A suite of tools called PCBoom [3] was used to generate the results.

PCBoom comprises a suite of computational tools that use full ray tracing to model sonic boom propagation, calculate ground boom signatures originating from flight vehicles performing arbitrary maneuvers, and assemble sonic boom footprints. The original version of PCBoom expanded on an early NASA sonic boom program written by Thomas [4] by adding focus boom prediction capability [5]. Although the first version of PCBoom modeled boom propagation for a single ray at a single flight condition, subsequent versions extended capabilities to handle vehicle maneuvers and several types of aircraft source input. Other modeling changes were also implemented, including handling signature aging via waveform steepening and shock fitting [6], support for specification of atmospheric conditions using several different formats, and inclusion of terrain data in ground intercept calculations. Additional modules can also be used for calculation of secondary booms and ray tracing of "over the top" booms [7], application of waveform filters to model turbulence effects using different methods [8–10], calculation of the effect of finite ground impedance on boom signatures, and calculation of signature propagation through focal zones using the Lossy Nonlinear Tricomi Equation (LNTE) [11–12]. Description of the latter capability is included as part of Section V, whereas use of the former modules is outside the scope of this paper.

The two PCBoom modules used for non-focus case propagation modeling are called FOBoom and PCBurg. FOBoom is the ray tracing and primary boom calculation program within PCBoom. Version 6.80b was used to generate results presented at SBPW3. A newer version, 7.0.1, includes support for higher resolution input data and was used to generate the final set of propagation case results reported in this paper. As will be shown, there was minimal difference between the two sets of results. PCBurg and its batch counterpart HeadlessBurgers are lossy propagation modules that use Burgers equation to model the effects of molecular relaxation on sonic boom signature evolution. Accounting for such effects is particularly important in modeling ground signatures to be used for calculating loudness metrics, such as Stevens Mark VII perceived level of loudness (PL) [13], because loudness levels can be strongly affected by molecular relaxation from propagation through humid atmospheres which manifests as changes to shock rise time. A typical application of these modules involves using FOBoom for ray tracing and generation of data files containing ray paths, ray tube areas, Blokhintzev and age parameters, and profiles of key atmospheric parameters (such as relative humidity) which are subsequently used by PCBurg for lossy propagation modeling. Parallel development of a Burgers equation propagation model within FOBoom by Lonzaga [14] has sought to improve upon the current model, and increase computational efficiency. This paper focuses on the legacy tools.

The SBPW3 propagation test cases required participants to model acoustic propagation from the near field of vehicles in steady level flight to specified ground elevations. Vehicle source characteristics were provided in the form of normalized pressure signatures versus axial distance, dP/P versus x, at many different azimuth angles φ comprising the lower half of pressure cylinders. Note that the azimuth convention used has $\varphi = 0°$ directly below the vehicle and negative azimuth angles toward the pilot's left side. Atmospheric conditions were provided in the form of profiles of temperature, pressure, two-dimensional wind, and relative humidity. Propagation Case 1 modeled a powered equivalent of the NASA C25D configuration that was used in SBPW2, called C25P. Starting pressure signatures for Case 1 were taken from computation fluid dynamics (CFD) results at a normalized radial distance $R/L = 3$, and those pressure data are shown in Figure 1(a). Propagation Case 2 modeled an early design version of NASA's Low Boom

Flight Demonstrator (LBFD) X-59 aircraft, called C609. Starting pressure signatures for Case 2 were also taken from CFD results at $R/L = 3$; Case 2 pressure data are plotted in Figure 1(b). As those figures show, the starting pressure signatures are generally complicated with significant azimuthal variation and multiple shocks making up a sawtooth pressure signature. In both cases, axial data ranges were sufficient to capture pre-shock ambient regions and to allow the pressure signatures to return to zero aft of the vehicle. Flight conditions and related parameters for the propagation cases are summarized in Table 1, where vehicle heading is defined as degrees clockwise from north and vehicle lengths were derived from supplied R/L values and dimensional starting radii.

Table 1. Summary of vehicle trajectory and modeling parameters for propagation cases

	Mach number	Flight altitude	Heading	Ground elevation	Starting R/L	Vehicle length
Case 1	1.6	51,706 ft	90°	866.4 ft	3.0	110 ft
Case 2	1.4	54,000 ft	90°	360.9 ft	3.0	90 ft

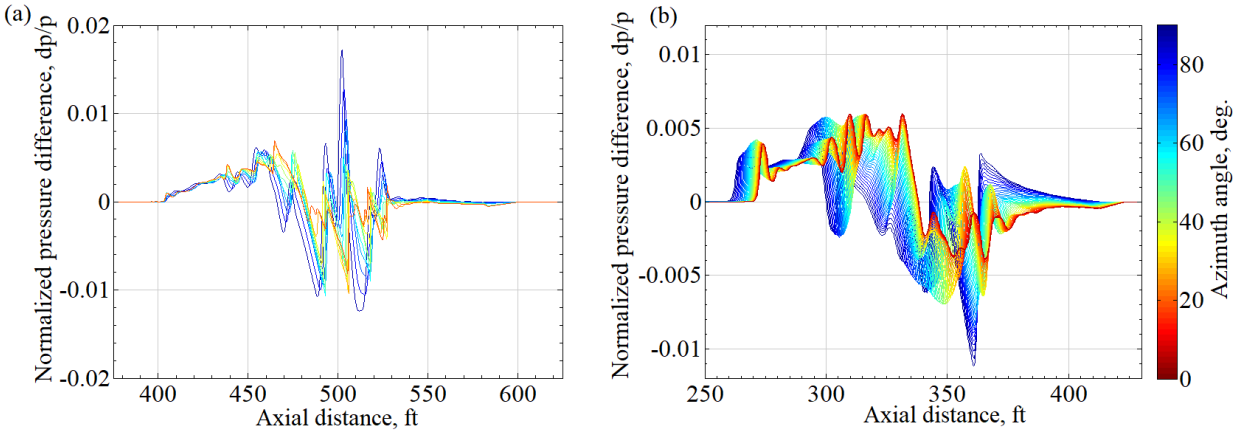

Figure 1. (a) Pressure signatures for propagation Case 1: C25P low-boom concept at $R/L = 3$, (b) Pressure signatures for propagation Case 2: LBFD Concept C609 at R/L = 3

Atmospheric profiles in each case were supplied at 39 levels from the ground to approximately 100,000 ft above flight altitude. Additionally, profiles describing temperature and pressure for the international standard atmosphere were used in Case 2 along with a specified relative humidity profile. The Case 1 and Case 2 atmospheric profiles represent deviations from standard conditions as illustrated in the profiles of Figure 2. Note that the wind direction convention is defined as the direction toward which the wind blows: a positive x wind is toward the east, and a positive y wind toward the north. In both cases there is a strong tailwind which is expected to produce wide sonic boom carpets. Wind profiles for both cases also include crosswinds which will make ray ground intersections and acoustic metrics asymmetric about the flight track. The Case 2 standard temperature and pressure profiles comprised eight levels, and SBPW3 instructions called for linear interpolation of pressures. PCBoom linearly interpolates atmospheric conditions. The Case 2 standard atmosphere temperature data were functionally equivalent to standard temperature lapse rates.

III. Propagation Modeling Methodology

A. General PCBoom propagation modeling

In addition to utilizing a built-in F-function library and user-supplied F-functions, PCBoom can also use pressure cylinders and axial dP/P profiles as source input. Due to non-uniform axial coordinates across azimuths in the supplied pressure data, line profiles of dP/P were used rather than pressure cylinders, and PCBoom was run one azimuth angle at a time[4]. The supplied near-field pressure data comprised relatively large numbers of axial stations, particularly in Case 1. To work within array limits in FOBoom 6.80b, dP/P profiles were downsampled prior to modeling. Due to multiple shocks and hence large variations in slope along the signatures, regular decimation of points would likely cause a loss of information such as local minima and maxima.

[4] FOBoom 6.80b does not require constant Δx in pressure cylinders, though it does require uniform axial coordinates at all azimuths. Newer versions of FOBoom can use cylinders with non-uniform axial coordinates across azimuths.

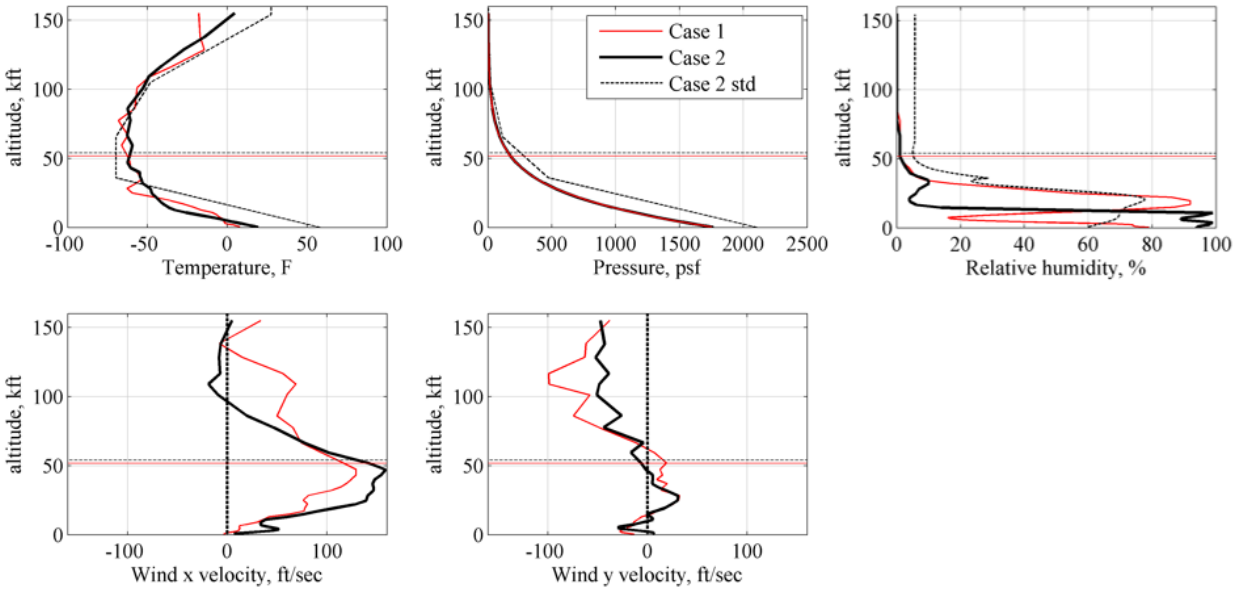

Figure 2. Atmospheric profiles for propagation Cases 1 and 2. Horizontal lines represent flight altitude in each case

Downsampling was done using a recursive endpoint fit algorithm known as the Ramer-Douglas-Peucker algorithm [15]. The principle behind that algorithm is that a set of points describing an arbitrary shape is down-selected by calculating the distance between the original shape and that described by the downsampled set of points. The maximum distance ε is a user-specified value and in this application ε was determined iteratively considering the final number of points in the signature. A comparison of $dP/P(x)$ in its original resolution to the downsampled resolution used in FOBoom 6.80b is shown in Figure 3(a). Examination of individual points in Figure 3(b) shows that the RDP algorithm tends to remove more points in linear portions of the pressure signature and retain points near peaks and curved sections. Following submission of results for presentation at SBPW3 a newer version of FOBoom (7.0.1), capable of handling high-resolution pressure inputs, was used to model propagation with full-resolution signatures. Comparisons of those results are the subject of section IV.C.

The PCBoom convention for wind direction is that components of wind are given in the engineering vector sense, rather than the meteorological sense, and are positive in the direction the wind is blowing toward. That is the same convention required by SBPW3 so no change was made to wind direction or sign. The PCBoom convention for azimuth angles is that zero degrees is directly under the aircraft, with positive azimuth angles toward the pilot's left side. The SBPW3 convention used the opposite, with negative azimuth angles toward the pilot's left side.

FOBoom includes an algorithm to find lateral cutoff angles automatically; alternatively users can specify azimuth angles to be modeled. In the course of modeling these cases, it was observed that the FOBoom algorithm produces lateral cutoff angles on the order of 0.5° smaller than those found manually by finely incrementing azimuth angles until doing so caused rays to refract away from the ground. As is shown in the results section, however, results in that region must be evaluated critically, as signatures were observed to be physically unrealistic at some extreme azimuth angles.

Following ray tracing calculations using FOBoom, propagation modeling with molecular relaxation effects was done using two Burgers equation tools with a common codebase: interactive PCBurg and the batch version HeadlessBurgers. Initial investigations were done using PCBurg for visual inspection of pressure signatures at 1,000 ft altitude increments. Subsequent analysis was done using HeadlessBurgers. Ray paths, ray tube areas, relevant atmospheric conditions, and starting signatures are passed from FOBoom to PCBurg/HeadlessBurgers. As a first step, PCBurg/HeadlessBurgers redistribute the starting pressure signatures onto evenly spaced grids at a user-specified sampling rate between 10 kHz and 102.4 kHz. An anti-Gibbs phenomenon filter is provided as a user option to condition pressure signatures at intermediate steps. Following propagation to the ground level, a reflection factor of 1.9 was applied before calculating metrics. Final results were modeled using a sampling rate of 102.4 kHz and default time-step factor 0.05, with the anti-Gibbs phenomenon filter applied.

In calculating PL for a sonic boom signature, consideration was given to how to handle energy from bow and tail shocks. For an ideal N wave with shocks separated by more than 70 msec (the time constant of human auditory response), the human ear will perceive two distinct events. Since the power spectral density calculated in the PL algorithm represents the full signature, the approach taken for this analysis was that the energy should be divided by two to account for perception of two distinct events [16]. The PL metric algorithm used in this work was validated by using the NASA Loudness Code for Asymmetric Sonic Booms (LCASB) [17] to calculate metrics from modeled signatures and verify consistent handling of energy level averaging.

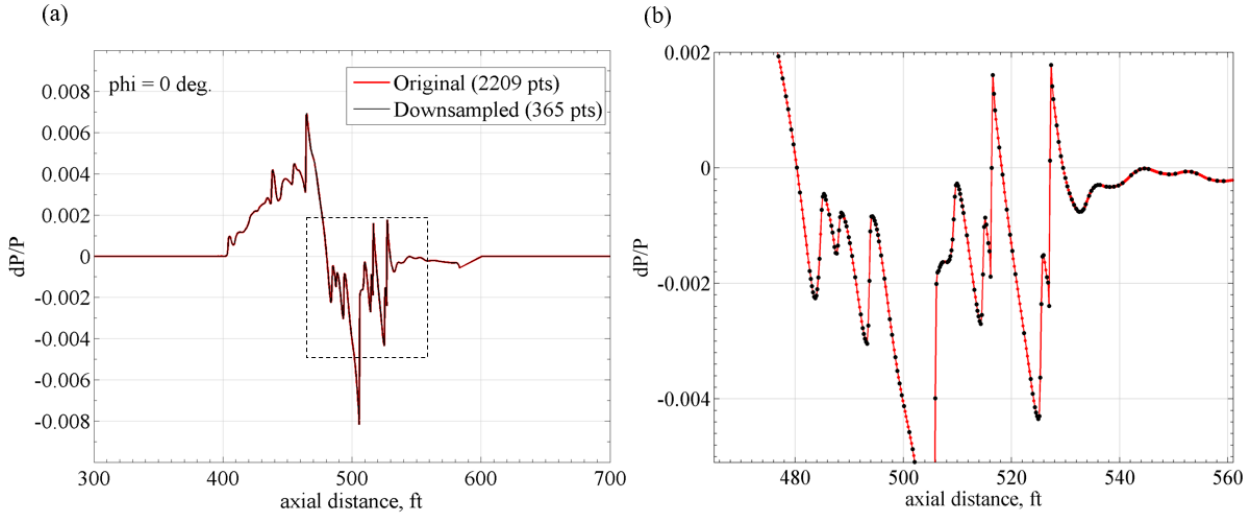

Figure 3. (a) Comparison of full-resolution starting pressure signature and downsampled signature, (b) magnified view of midbody shocks

B. Focus handling in PCBoom

PCBoom has the ability to predict the location and extent and sonic boom signatures in focal zones as is created by arbitrary, dynamic, maneuvering flight and from the diffraction of rays due to atmospheric gradients based on the method developed by Plotkin and Cantril [5]. FOBoom calculates the focal zone, ray tracing, and geometric parameters such as caustic curvature and diffraction boundary-layer thickness. For greater investigative detail on the focus rays, an interactive module RayCau visualizes the selected rays from FOBoom with respect to the ground, and computes several additional parameters, such as the ray elevation angle. Focused waveforms near the centerline may also be predicted using the 2D Lossy Nonlinear Tricomi Equation LNTE [12, 18]. Molecular relaxation of the LNTE input signature was conducted in PCBurg. The LNTE output signatures were used to calculate loudness metrics with LCASB [17].

C. Description of lossy nonlinear Tricomi equation method

The LNTE module developed by Salamone [12] and implemented in PCBoom, determines a numerical solution to the lossy nonlinear Tricomi equation (eq. 1) when provided an incoming waveform, acoustic parameters, and an atmospheric profile.

$$\frac{\partial^2 p}{\partial \bar{z}^2} - \bar{z}\frac{\partial^2 p}{\partial \bar{t}^2} + \frac{\beta}{\varepsilon^2 \rho_0 c_0^2}\frac{\partial^2 p^2}{\partial \bar{t}^2} + \left(\frac{\bar{\alpha}}{\varepsilon^2} + \sum_{v=1}^{2} \frac{\bar{\theta}_v / \varepsilon^2}{1 + \bar{\tau}_v \dfrac{\partial}{\partial \bar{t}}} \right) \frac{\partial^3 p}{\partial \bar{t}^3} = 0 \qquad (1)$$

Development of LNTE as part of a larger flight test program is described in detail in the work by Page *et al.* [11] and summarized here. The first two terms in the Tricomi equation account for diffraction, the following term encompasses nonlinearity, and the final term represents thermoviscous and relaxation effects. The code iteratively solves for the solution to this equation from an initial guess by adding an unsteady pressure term and a pseudotime variable, σ (eq. 2).

$$\frac{\partial^2 p}{\partial\sigma\partial\bar{t}} = \frac{\partial^2 p}{\partial\bar{z}^2} - \bar{z}\frac{\partial^2 p}{\partial\bar{t}^2} + \frac{\beta}{\varepsilon^2\rho_0 c_0^2}\frac{\partial^2 p^2}{\partial\bar{t}^2} + \left(\frac{\bar{\alpha}}{\varepsilon^2} + \sum_{v=1}^{2}\frac{\bar{\theta}_v/\varepsilon^2}{1+\bar{\tau}_v\dfrac{\partial}{\partial\bar{t}}}\right)\frac{\partial^3 p}{\partial\bar{t}^3} \tag{2}$$

The pseudotime variable is unrelated to the dimensionless time variable, $\bar{t}$. The dimensionless time is given by $\bar{t} = f_{ac}t$, which represents the time delay, scaled by the characteristic acoustic frequency, f_{ac}. The dimensionless vertical distance, $\bar{z}$, in the above equations refers to a ratio of the physical distance, z, from the caustic to the diffraction boundary-layer thickness, in the normal direction (eq 3).

$$\bar{z} = z\left[\frac{R_{tot}c_0^2}{2f_{ac}^2}\right]^{\frac{1}{3}} \tag{3}$$

According to this relationship, if the pressure variable in eq. 1 was normalized by a characteristic acoustic pressure, P_{ac}, the coefficient in the third term of eq. 1 would be presented as follows:

$$\frac{\mu}{2} = \frac{\beta P_{ac}}{\varepsilon^2\rho_0 c_0^2} = \frac{\beta P_{ac}}{\rho_0 c_0^2}\left[\frac{R_{tot}f_{ac}}{2c_0}\right]^{\frac{2}{3}} \tag{4}$$

The variable μ in eq. 4 represents the magnitude of the nonlinear effects relative to the diffraction effects. P_{ac} is typically set to the peak amplitude value of the incoming waveform at $\bar{z} = 1$.

Figure 4 illustrates the focusing condition modeled by the Tricomi equation. This process affords one the observance of the alteration of an incoming wave near the caustic, including the amplitude and phase changes as it passes through the caustic, as well as the signature that propagates into the shadow zone.

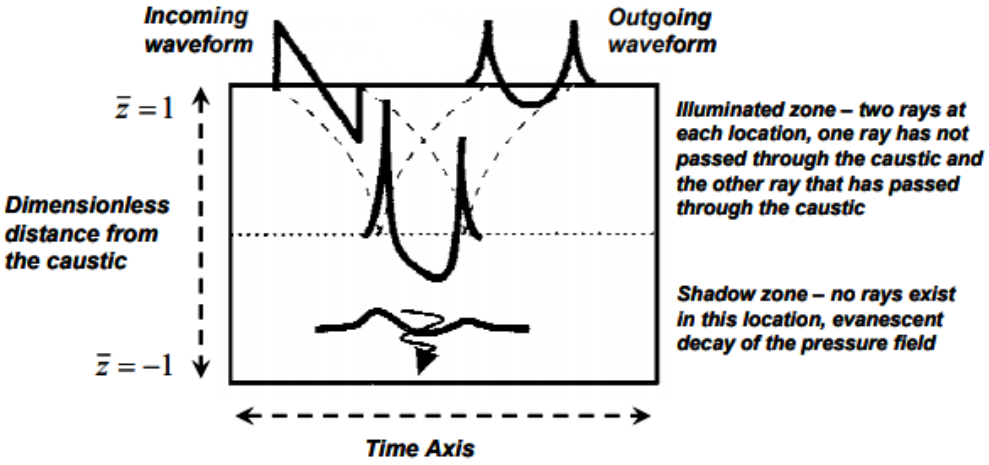

Figure 4. Depiction of the focus condition [19] modeled by the Tricomi code (Reproduced from Ref. [12] by Salamone)

D. Burgers-LNTE Interface

The ray path geometry must be understood in order to locate the focus delta ray. Figure 5 indicates that the light blue caustic line is parallel to the purple line depicting $\bar{z} = 1$. These lines are separated by the orange orthogonal line of length delta (δ), which refers to the diffraction boundary-layer thickness. The focus delta ray is illustrated by the dark blue line with the new Mach conditions. Advancing the aircraft trajectory time in FOBoom to select the ray that passes through the calculated Burgers-LNTE interface point, rather than an assumed ground intersection point, accounts for the true curvature of the focus delta ray path.

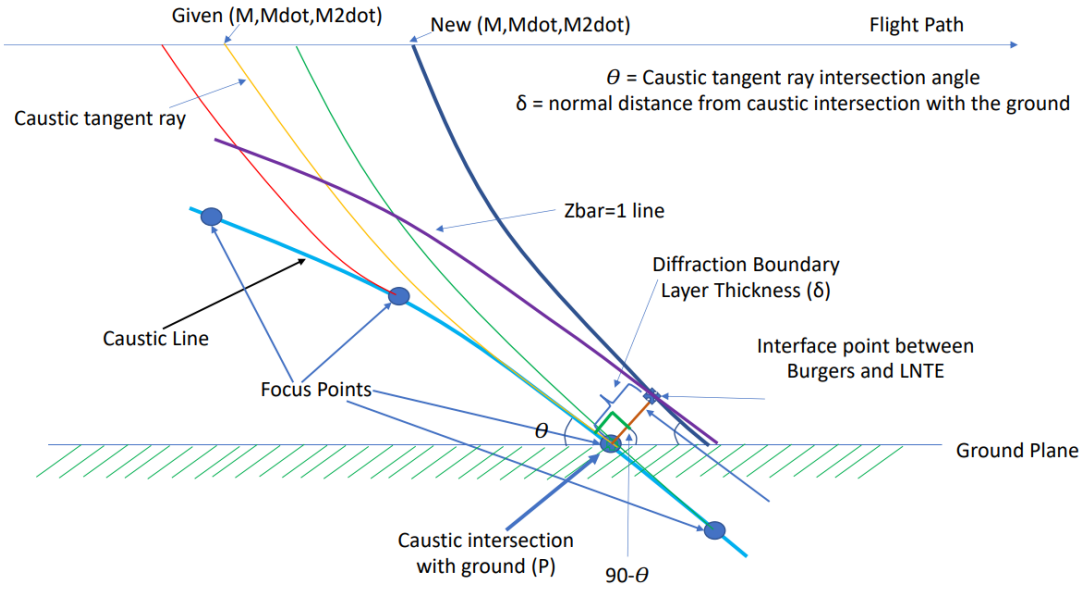

Figure 5. Geometric interface between ray tracing and LNTE (Reproduced from Ref. [20] by Rallabhandi)

This interface location is where ray tracing meets the Tricomi code, and is therefore where the pressure signature must be extracted from PCBurg in order to be fed into LNTE. Figure 6 illustrates the exact coordinates of the extraction point. Note that the orange diffraction boundary-layer thickness begins at the caustic ground intersection point, and terminates at the Burgers-LNTE interface point at altitude $z = \delta\cos(\Theta)$ + ground plane height. The focus delta ray intersects the Burgers-LNTE interface point at a distance $x = \delta\sin(\Theta)$ greater than the caustic ground intersection point.

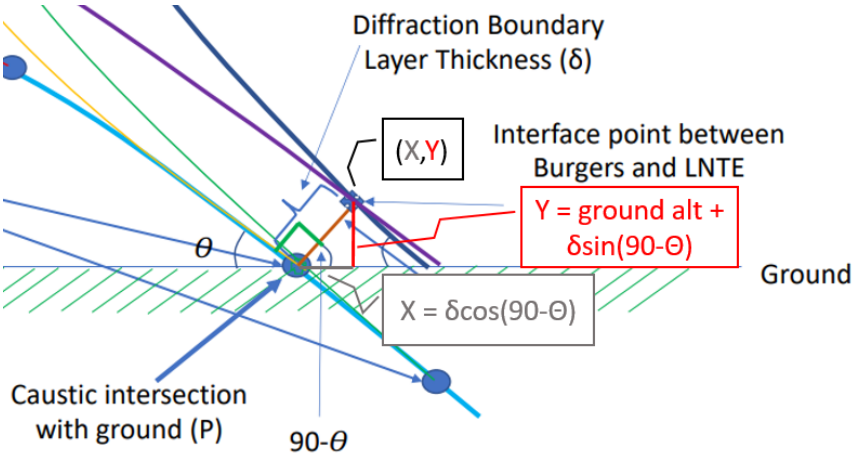

Figure 6. Coordinates of geometric interface between ray tracing and LNTE

Figure 7 demonstrates the discrepancy between signatures calculated with different ray path assumptions. Although similar, the signature (shown in blue) from the approximated straight ray path predicts slightly lower peak overpressure than the signature (shown in red) computed with the more accurate, curved ray path. This phenomenon is consistent among all signatures calculated using LNTE at $\overline{z} = -1$, 0, and 1. This ray path geometry was not fully understood until after initial submittal of results to SBPW3, therefore the results discussed in section V.B. do not properly locate the focus delta ray. A comparison of the incorrect ray with the revised solution submitted in March 2020 which properly identifies the focus delta ray and accurately locates the Burgers-LNTE interface can be found in section V.C.

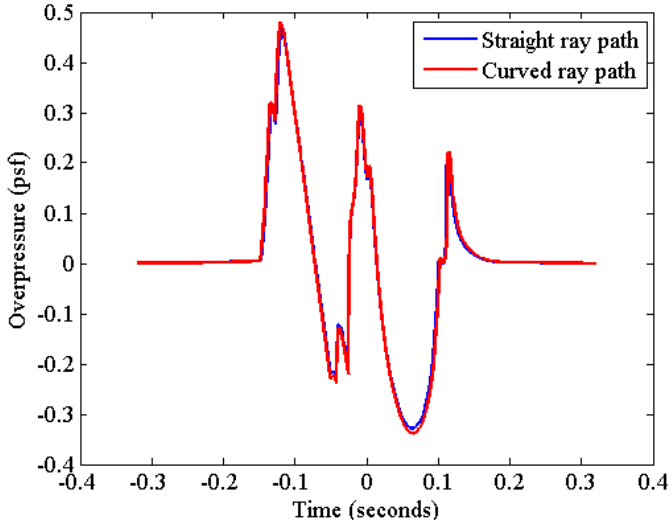

Figure 7. Ray path signature comparison at $\bar{z} = 1$

Because the Burgers-LNTE interface point is not located at the ground, computing the focus delta ray requires concatenation of PCBurg outputs from parallel batch scripts. One script identifies the ground at its true, physical altitude, while the other sets the ground at the Burgers-LNTE interface altitude. The former is required in order to account for the caustic curvature and diffraction boundary-layer thickness, which can currently only be calculated using near ground height inputs. The latter is required in order to terminate propagation in PCBurg at the desired altitude to extract and feed the output signature into LNTE. This process is required because PCBurg output signature altitude is currently restricted to even multiples of 1,000 ft and a ground height specified in FOBoom. Future development of PCBoom detailed in section VI could eliminate the need for parallel run streams.

IV. Results: Propagation Cases

The SBPW3 propagation case results primarily comprise pressure signatures at the ground, calculated ground metrics, and ground ray intersection locations. Results in this section represent non-focus cases. Complete tables of ground metrics are included in the appendix. Results of the optional focus case are given in section V.

A. Case 1 results

The modeled sonic boom carpet from the NASA C25P flying at Mach 1.6 and altitude 51,700 ft was fairly wide in the azimuthal sense, spanning nearly 150°. Due to the crosswind component of the atmospheric profile, the lateral cutoff angles were asymmetric with right lateral cutoff at $\varphi = 69.0°$ and left lateral cutoff at $\varphi = -78.3°$. A progression of boom signatures at several intermediate altitudes is shown in Figure 8, with the bottom signature representing the ground signature before application of the 1.9 reflection factor. Shock coalescence required a large altitude range in this case, with some of the shocks which originated from the aft portion of vehicle still recognizable at 10,000 ft. The ground signature appears comparatively smooth with a long rise time to the bow shock which suggests a dominance of low frequency components. The long rise time also contributes to a lower PL than that which could be expected from a sharply rising N-wave signature.

Ground metrics across the span of the carpet are plotted in Figure 9. The azimuthal distributions of metrics are relatively flat in the middle of the carpet, with local maxima at locations near $\varphi = \pm 30°$. The maximum PL is approximately 75 PLdB, which has been characterized as a "sonic thump" and similar in loudness as a car door slamming. Near lateral edges of the carpet, metric levels decrease sharply. Among metrics considered for SBPW3, the largest variation in level across the carpet occurs for PL. Ground intersection points for rays in 10-degree increments were plotted in Figure 10 and show that the modeled physical carpet width was approximately 24.9 nm. The aircraft heading in this case was 90°, or in the positive x direction. Asymmetry of ground locations about the flight track is evident and comparing discrete points it appears that much of that asymmetry arises at high azimuth angles. The wind profiles in Figure 2 show that there were regions of both left and right crosswinds in the y-wind profile, thought left crosswinds show slightly larger maximum magnitude and cover a wider range of the profile below the flight altitude. Thus, it appears that the cumulative effect is to blow left-side rays farther off-track than the right-side rays.

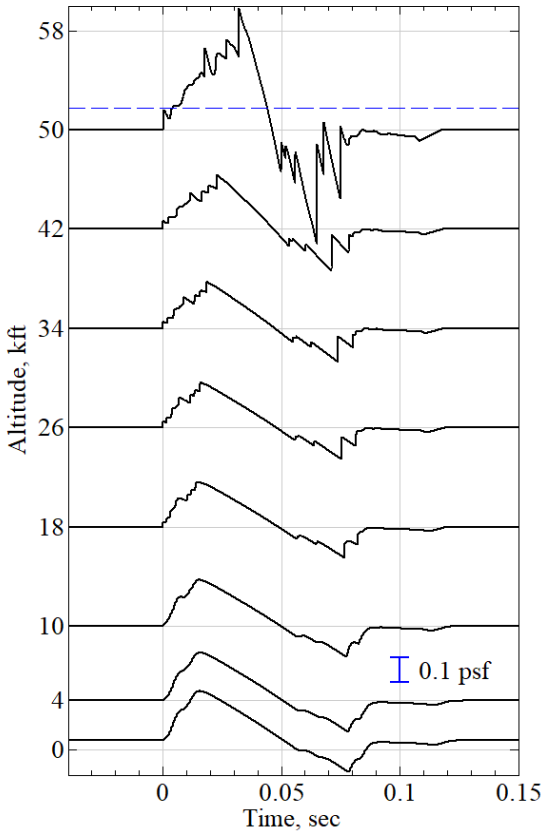

Figure 8. Case 1 undertrack pressure signatures at intermediate altitudes; horizontal dashed line indicates flight altitude

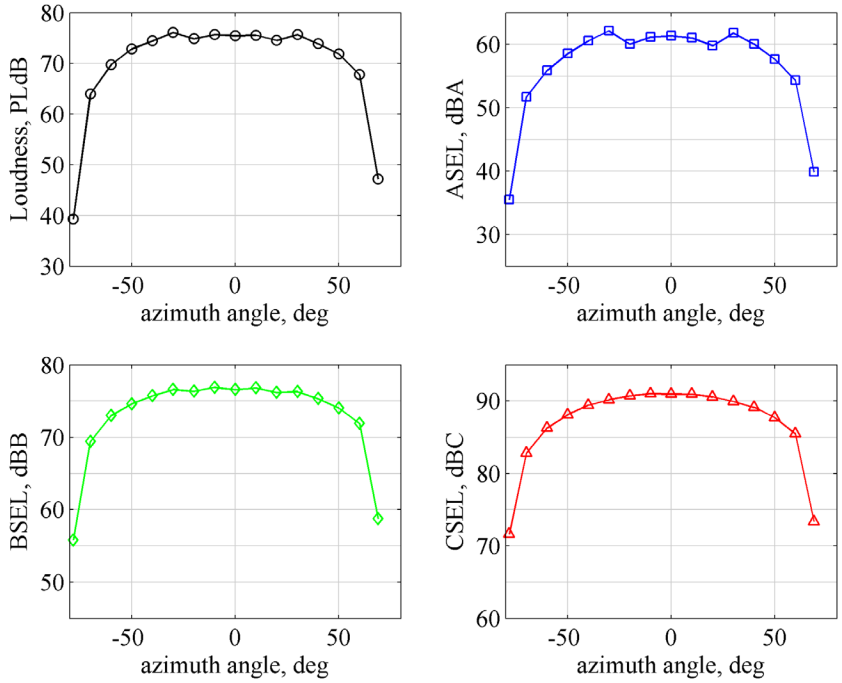

Figure 9. Metrics calculated from Case 1 ground signatures

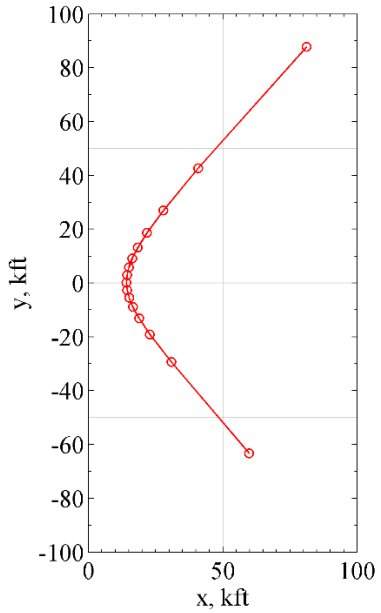

Figure 10. Ground intersections for Case 1 rays

B. Case 2 results

The sonic boom carpet from the C609 vehicle flying at Mach 1.4 and altitude 54,000 ft was wide in the azimuthal sense, spanning 134.4°. When a standard atmospheric profile with no winds was used, however, the azimuthal carpet width was slightly less than 90°. The wind profiles in Figure 2 show that the non-standard Case 2 atmosphere had the vehicle flying with a strong tailwind which contributed to the carpet width differences: 20.1 nm versus 9.2 nm for the standard no-wind atmosphere. Due to the crosswind component of the atmospheric profile, the lateral cutoff angles were asymmetric with right lateral cutoff at $\varphi = 70.5°$ and left lateral cutoff at $\varphi = -63.9°$, versus symmetric lateral cutoff angles of ±44.8° for the no-wind case. A progression of boom signatures at several intermediate altitudes is shown in Figure 11, with the bottom signature representing the ground signature before application of the 1.9 reflection factor. Those profiles show that shocks do not completely coalescence and some features in the ground signature can be attributed to mid-body shocks in the near-field signature. As with Case 1, the ground signature has a long ramp to the peak overpressure which suggests a dominance of low frequency components.

Ground metrics across the span of the carpet are plotted in Figure 12. The azimuthal distributions of metrics are relatively flat in the middle of the carpet, with local maxima in PL and ASEL at locations near $\varphi = \pm 30°$. The maximum PL is 77.6 PLdB at an azimuth angle of 30°. Near lateral edges of the carpet the metric levels decrease sharply, and this is a case in which an extreme lateral cutoff angle was deemed unrealistic. FOBoom ray tracing results showed that a ray originating at −64.0° would intersect the ground. Lossy propagation modeling showed that the loudness of the ground signature from that ray was 28.6 PLdB versus 41.8 PLdB for a ray just 0.1° lower in azimuth. Inspection of ray paths also showed large differences that indicated a large influence of limited numerical precision within the code and, as a result, −63.9° was taken as a more reasonable lateral cutoff angle. Ground intersection points for rays in 10-degree increments are plotted in Figure 13. The aircraft heading in this case was 90°, or in the positive *x* direction. As in Case 1, asymmetry of ground intersection locations about the flight track is evident with larger left/right differences at higher azimuth angles. The wind profiles in Figure 2 show that there were regions of both left and right crosswinds in the *y*-wind profile, with left crosswinds occurring in a band of altitudes above the band of altitudes associated with right crosswinds.

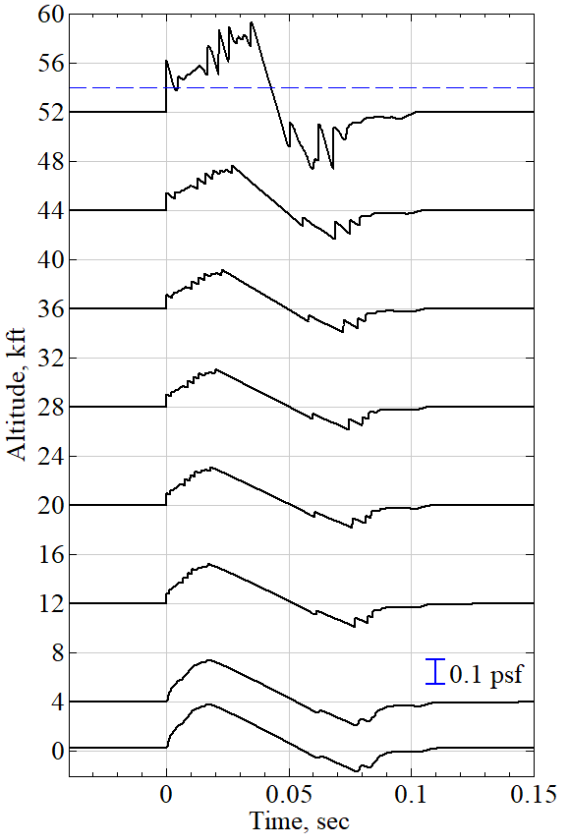

Figure 11. Case 2 undertrack pressure signatures at intermediate altitudes, with flight altitude indicated by a horizontal dashed line

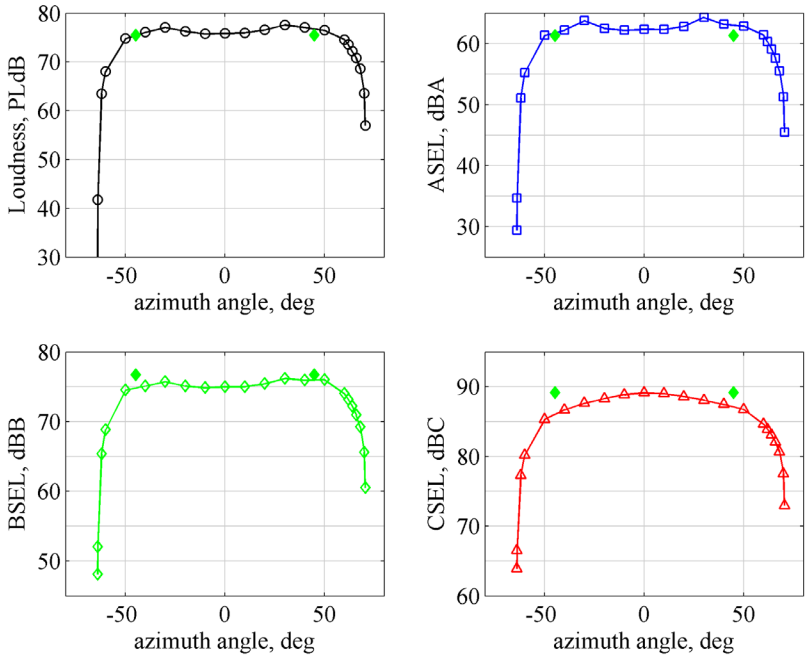

Figure 12. Metrics calculated from Case 2 ground signatures. Solid green diamonds represent metrics at lateral cutoff (φ = ± 44.8°) in the standard atmosphere case

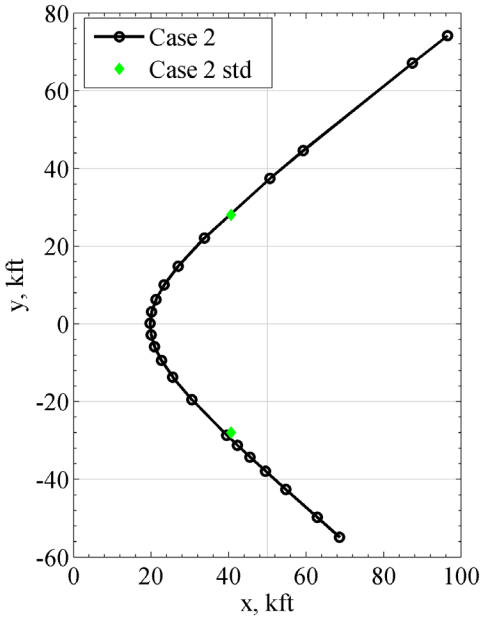

Figure 13. Ground intersections for Case 2 rays. Solid diamonds represent lateral cutoff locations in the standard atmosphere case

C. Comparison of results from FOBoom 6.8b and FOBoom 7

Results presented at SBPW3 were modeled using FOBoom 6.8b, which necessitated downsampling of starting pressure signatures. As part of FOBoom 7.0.1 development and testing, the SBPW3 propagation cases were modeled using full resolution starting signatures making use of a new high resolution capability in FOBoom 7. Keeping all other parameters such as HeadlessBurgers sampling rate fixed, differences in results from using the two sets of input data were generally small. Maximum overpressures and ground signature metrics for example rays from each case are summarized in Table 2. Metric differences are within hundredths of a dB, and maximum over pressure differences are likewise small. Modeled ground signatures were compared in Figure 14(a), with a magnified view of the peak overpressure in Figure 14(b). Given that starting pressure signatures in the Burgers equation solver are resampled onto a uniformly spaced time series using linear interpolation, and that the signature downsampling method was based on minimizing deviation from the original signature, it can perhaps be expected that the final differences would be small.

Table 2. Comparison of ground signature metrics modeled with FOBoom 6.80b (downsampled starting signatures) and FOBoom 7.0.1 (full resolution starting signatures)

Case		Pmax (psf)	PL	ASEL	BSEL	CSEL
Case 1, φ = 20°	FOBoom 6.80b	0.34512	74.6	59.86	76.20	90.60
	FOBoom 7.0.1	0.34510	74.6	59.83	76.20	90.60
Case 2, φ = −60°	FOBoom 6.80b	0.08542	68.1	55.24	68.84	80.23
	FOBoom 7.0.1	0.08542	68.1	55.23	68.84	80.23

D. Lossy propagation modeling with HeadlessBurgers: effects of sampling rate and time-step parameter

Sonic boom waveforms in PCBurg / HeadlessBurgers are represented as pressure series at uniform finite sampling rates. The waveform sampling rate is a user-selectable parameter, and values of 10, 25.6, 51.2, and 102.4 kHz are available in the current version of those tools. An investigation into sampling rate effects on waveform evolution and ground metrics was done as part of this shaped boom analysis. Figure 15 shows the effect on PL, ASEL, BSEL, and CSEL of signatures propagated to the ground using different sampling rates for a selection of azimuth angles. PL and ASEL appear more sensitive to differences in sampling rate, though for each metric and azimuth combination the levels converge to within a few tenths of a dB between 51.2 kHz and 102.4 kHz.

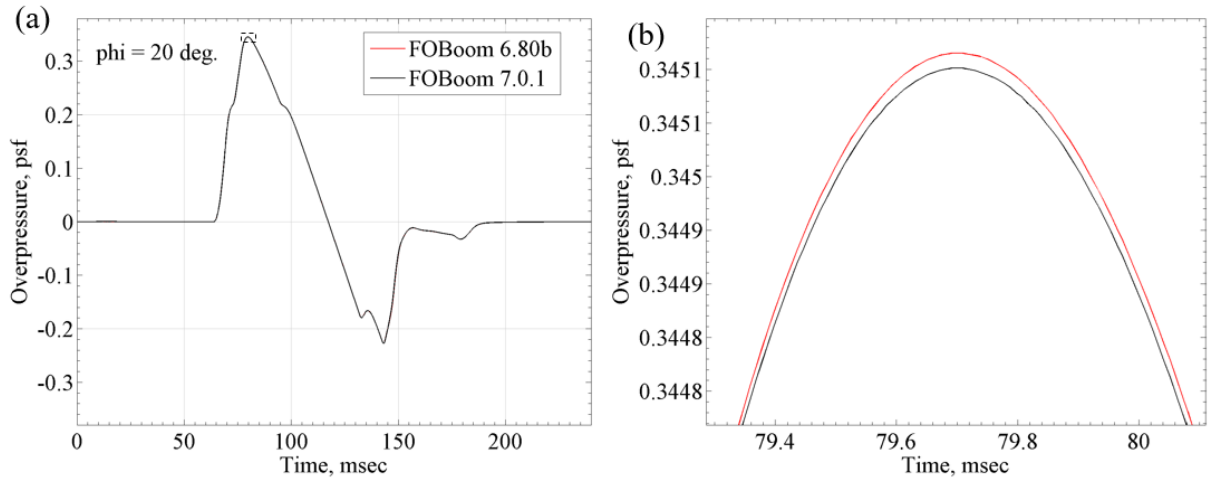

Figure 14. (a) Example ground signature comparison between FOBoom 6.80b (downsampled starting signatures) and FOBoom 7.0.1 (full-resolution starting signatures), (b) magnified plot of maximum overpressure

The differences between results modeled using sampling rates 51.2 kHz and 102.4 kHz were examined in more detail. Figure 16 displays the Case 1 and Case 2 differences in ground metrics using those two sampling rates. Delta metrics refers specifically to metric levels modeled using 102.4 kHz minus those modeled using 51.2 kHz.

Several phenomena can be observed from this comparison. Figure 16(a) illustrates an approximately symmetric delta between loudness metrics on either side of the vehicle in Case 1, across the φ = 0° axis. At the negative lateral cutoff angle there is larger delta in PL though other metrics calculated using those signatures are much closer between the two sampling rates. Note that BSEL and CSEL are the more consistent metrics between both sampling rates, exhibiting no clear outliers throughout the entire carpet. This is likely due to the smaller weighting adjustments on the low-frequency predicted boom content, compared to A-weighting scales. Overlaid ground signatures at −78.3° modeled with several sampling rates are shown in Figure 17. The larger delta for loudness can be explained by the ground signatures at that azimuth angle displaying a small deviation near the second shock (around 120 msec in Figure 17) between those calculated with either sampling rate. Ground signatures at other azimuths throughout the carpet are generally more consistent between sampling rates; an example is shown in the Figure 18 signatures at azimuth angle 0°. In that case, ground signatures appear consistent, though on a magnified scale some small differences can be observed in peak levels particularly for the difference between the minimum (10 kHz) and maximum (102.4 kHz) sampling rates.

The metric results for Case 2, modeled using different sampling rates, are similar to those for Case 1 and are shown in Figure 16(b). Metric deltas between the two sampling rates are typically between 0 and 0.2 dB. Figure 16(b) illustrates a single PL outlier with a delta of 1.6 PLdB at the extreme left lateral cutoff location, corresponding to an azimuth angle of −64.0°. Recall that results from that azimuth angle were deemed unrealistic and −63.9° was taken as the functional lateral cutoff angle. In that case the metric level that is low enough that it would likely be below ambient levels, and a small numerical difference in the waveform introduced by finite sampling rate can have a large effect on the metric level.

Propagation modeling in HeadlessBurgers uses discrete steps in time along the ray. The time step size is determined internally based on the propagation time at which the steepest segment in the signature would become vertical. That propagation time is multiplied by a time-step factor whose value is less than one. The default value of the time-step factor is 0.05, a value which was noted [3] as a good balance between computational speed and stability. A smaller time step factor of 0.002 was used to produce results for the original submission. Subsequent investigation showed that the resulting ground signatures exhibited small oscillations in pre-shock ambient levels. An example comparison of signatures modeled using time-step factors of 0.002 and 0.05 is illustrated in Figure 19. The pre-shock ambient portion of the signature is shown in Figure 19(b) with a magnified vertical scale. The effect of those oscillations on signature metrics is to generally raise the levels on the order of 0.5 dB or less, with some additional sensitivity at low levels near lateral cutoff. Following SBPW3, results were recalculated using a time-step factor of 0.05 and resubmitted during the permitted revision period. Results documented in this paper also represent those recalculated using a time-step factor of 0.05.

It is hypothesized that the oscillations may have been caused by the anti-Gibbs phenomenon filter at non-default time steps. That is, the filter may have been optimized for the default time-step size. Further investigation is required to fully understand the underlying cause of the pre-shock ambient oscillations.

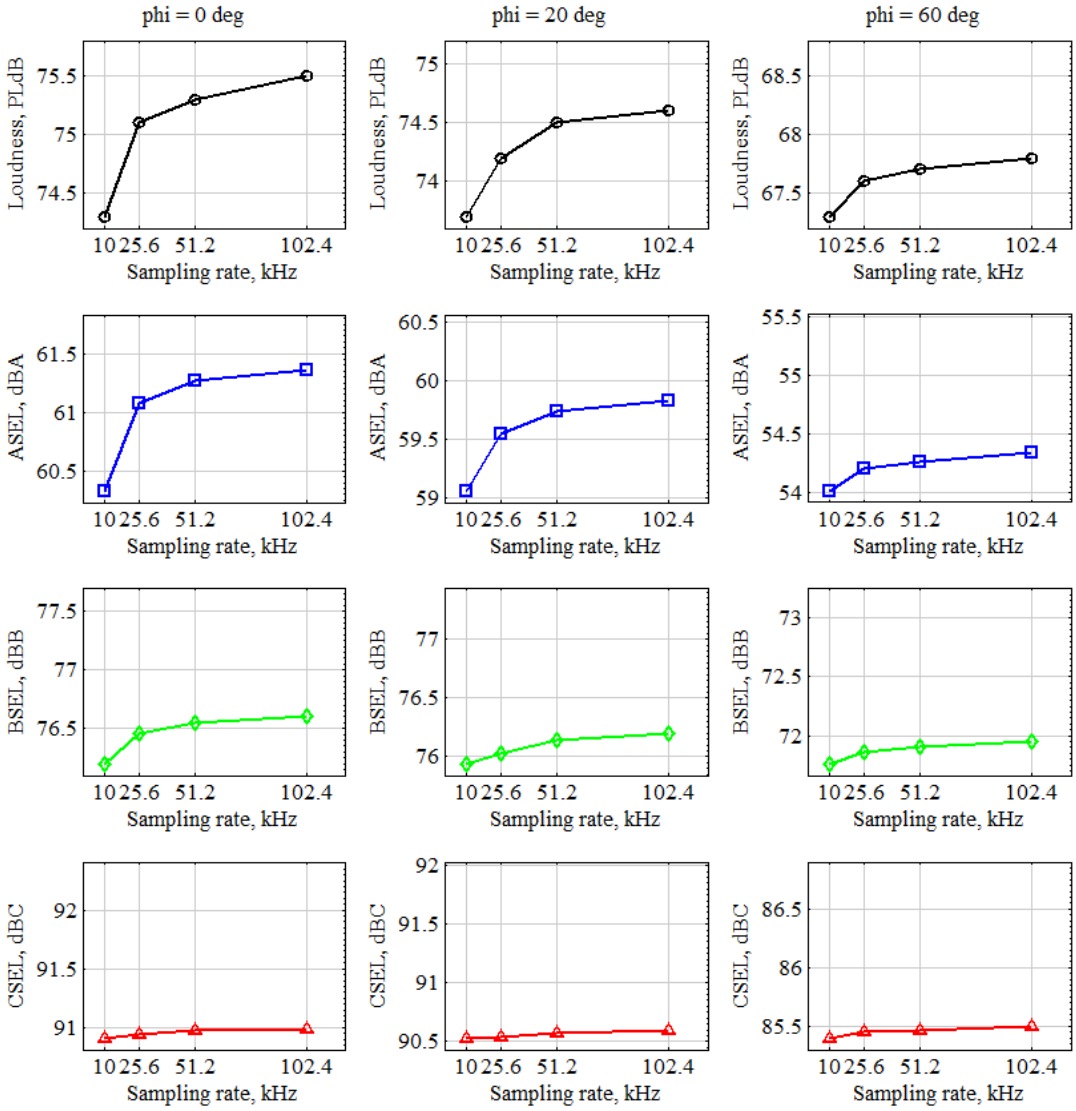

Figure 15. Results of Case 1 sampling rate study: columns from left to right represent undertrack ray, off-track ray, and ray near lateral cutoff; all plots have a vertical scale spanning 1.6 dB

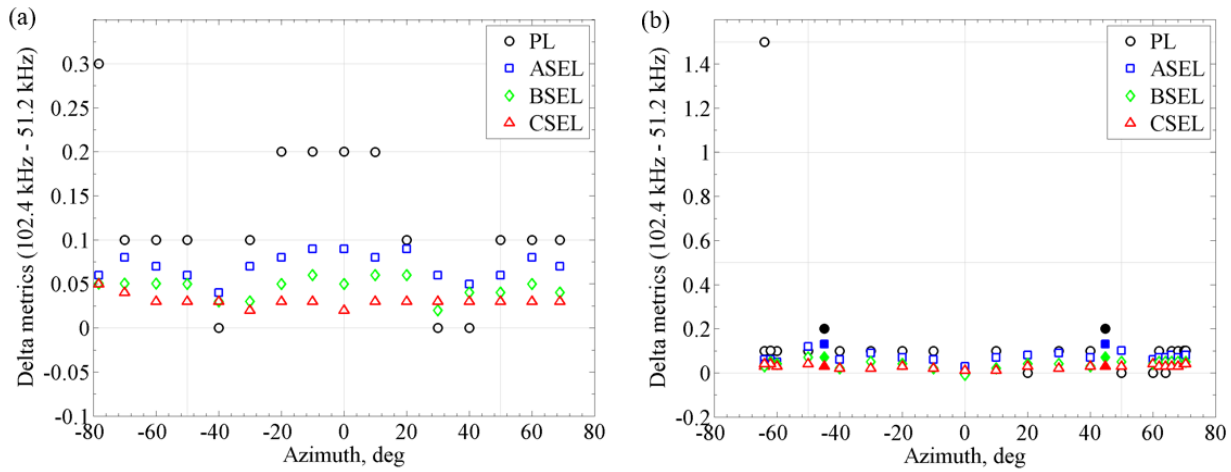

Figure 16. Differences in metrics levels from propagation modeling at 102.4 kHz versus 51.2 kHz for (a) Case 1, and (b) Case 2 (solid points at φ = ± 44.8° represent standard atmosphere conditions)

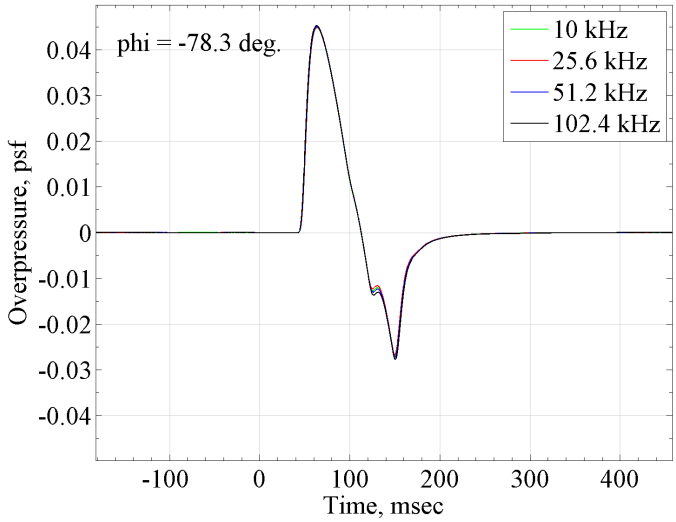

Figure 17. Ground signatures for Case 1, left-side lateral cutoff ray modeled using different sampling rates

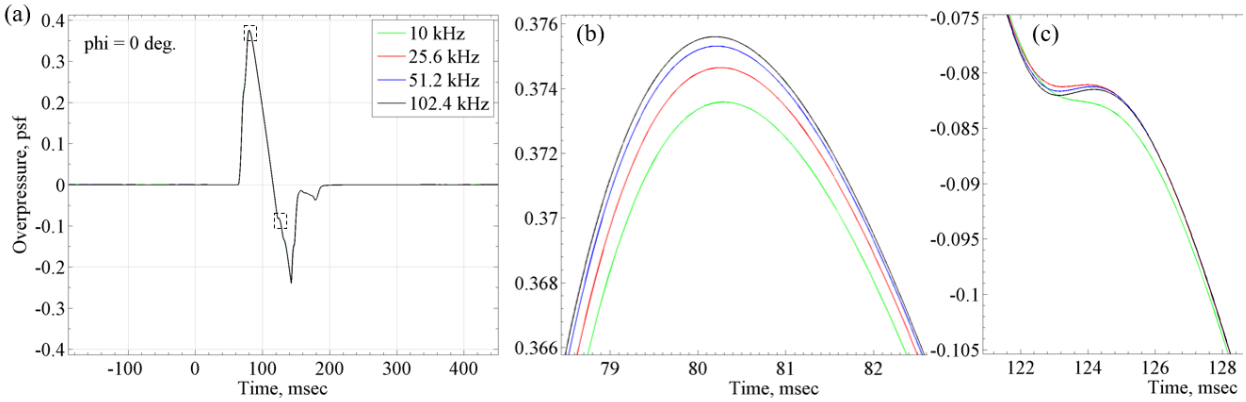

Figure 18. Ground signatures for Case 1 undertrack ray (a) with magnified insets showing (b) peak overpressure (c) midbody region

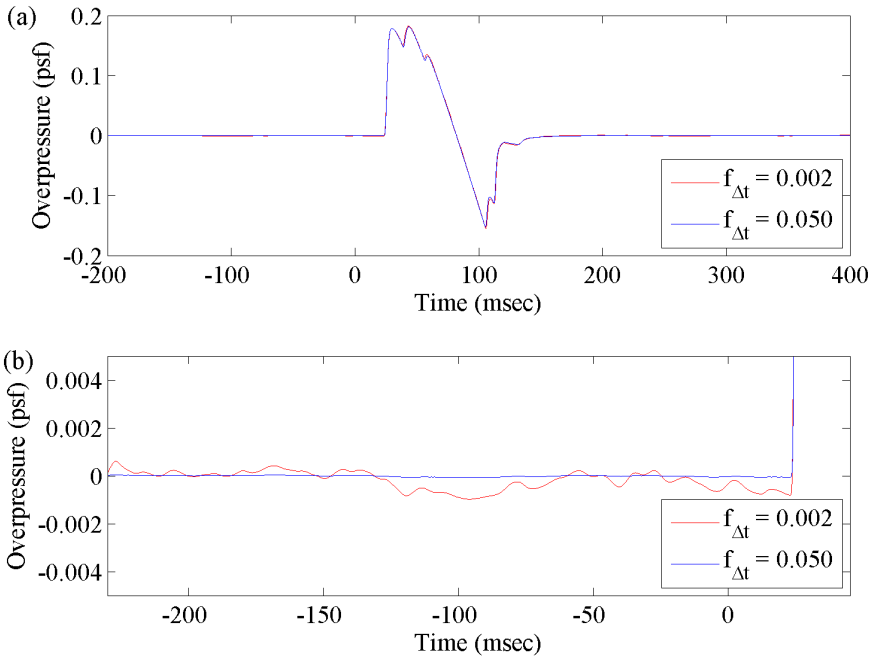

Figure 19. (a) Comparison of ground signatures for Case 2, φ = 50° modeled using two different time-step factors, (b) pre-shock ambient portion of signatures

V. Results: Focus Case

Evaluation of the Focus case was an evolving process. The initial analysis conducted in September identified some questions regarding the proper interface between FOBoom, PCBurg, and LNTE. Working closely with NASA and others yielded the interface diagram in Figure 5 and subsequent refinement of the interface process in early 2020. This section describes the nuances of the PCBoom-LNTE interface details and the evolution of the process.

A. LNTE parameter determination

In addition to outlining the fundamental methodology detailed in section III.B, much of the work leading up to the original submission in September 2019 consisted of an investigation of the LNTE convergence parameters. In doing so, three command line options were analyzed for optimal convergence: maximum pseudotime value, maximum sampling rate, and number of z-axis layers.

The version of the Tricomi code employed in this analysis does not have fixed convergence measures. Therefore, it was established that once the parameters exhibited reduction by at least four orders of magnitude, and minimal change was observed in solutions at several z-axis layers, sufficient convergence had been achieved. The three convergence parameters investigated were as follows:

- Normalized infinity norm of the top $\overline{z}$ with respect to the previous step
- Normalized infinity norm between successive iterations along the time history at the $\overline{x}$ location corresponding to the largest change in the nonlinear step
- Normalized infinity norm of the spectral amplitudes between successive iterations along the $\overline{z}$ axis corresponding to the largest change in the diffraction/absorption/dispersion step divided by the pseudotime increment

The parameterization analysis concluded that the LNTE input parameter values in Table 3 ensure optimal solution convergence.

Table 3. Final LNTE input parameters

maximum pseudotime value	maximum sampling rate (Hz)	Number of z-axis layers
18.0	24,000	4000

B. Results submitted 30 September 2019

The same LNTE input parameters were employed for all solutions discussed in this paper. Figure 20 displays the pressure vs. time signatures at each of the specified $\overline{z}$ locations: 1, 0, and −1, respectively. Note that the Burgers-LNTE interface discussed in section III.D was not properly identified during the computation of these results, hence the larger than expected peak overpressures for all three signatures. More information on the evolution of the ray geometry assumptions throughout the various iterations of the focus solution will be discussed in the following sections.

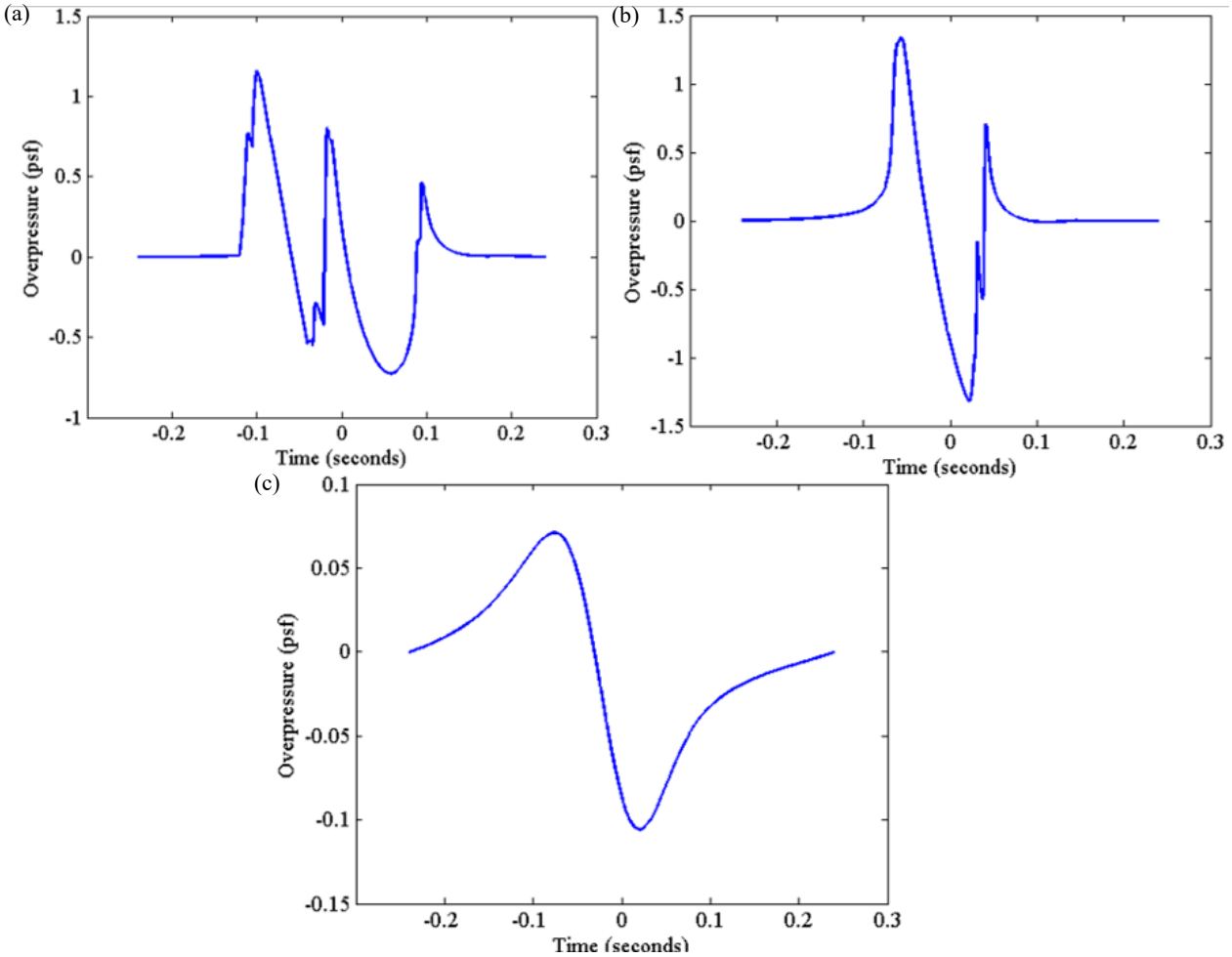

Figure 20. September submittal signatures at $\overline{z}$ = (a) 1, (b) 0, and (c) −1

Despite the overestimation of the overpressure, the general shape of each signature matches the expected results depicted in Figure 4**.** The outgoing waveform in the illuminated zone at $\overline{z}$ = 1 in Figure 20(a) exhibits the coalescence of both the N and U-shaped waveforms. The waveform closest to the caustic location $\overline{z}$ = 0 in Figure 20(b) includes only the single U-shaped waveform. The waveform behind the caustic in the shadow zone at $\overline{z}$ = −1 in Figure 20(c) demonstrates a heavily attenuated N-wave with rounded shocks and very low peak overpressure.

C. Refinement of method in January – March: focus delta ray location

As mentioned in section III.D, the solution submitted in September did not properly capture the focus delta ray geometry shown in dark blue in Figure 5. Note that Figure 5 was not developed until February 2020, and Figure 6 was not developed until April 2020, when these concepts were fully understood. Further investigation revealed that the original submission instead represented the caustic tangent ray, illustrated in yellow. The ray discrepancy was caused by the original solution not accounting for the advanced trajectory time describing the focus delta ray with corresponding updated Mach conditions. In addition to the trajectory advancement, the exact location of the Burgers-LNTE interface was determined for the revised solution. The ray tracing was corrected accordingly to pass

through the interface location, at which point the signature was extracted for input to LNTE. Note that the same LNTE input parameters as described in Table 3 were employed for all focus solution refinements discussed throughout section V.

Figure 21 compares the pressure vs. time signatures for the caustic tangent ray and the focus delta ray at each of the specified $\bar{z}$ locations: 1, 0, and −1, respectively. It is evident that the caustic tangent ray overestimates the peak overpressure predicted with the focus delta ray. The caustic tangent ray was extracted from PCBurg into LNTE at the true ground height where the Blokhintsev parameter sharply increases, causing the metrics and ground signatures to increase at lower altitudes. All future solution modifications discussed in this paper, including the final submitted results, are refined versions of the focus delta ray illustrated by the red curves in the following figure, with the significantly lower peak overpressure.

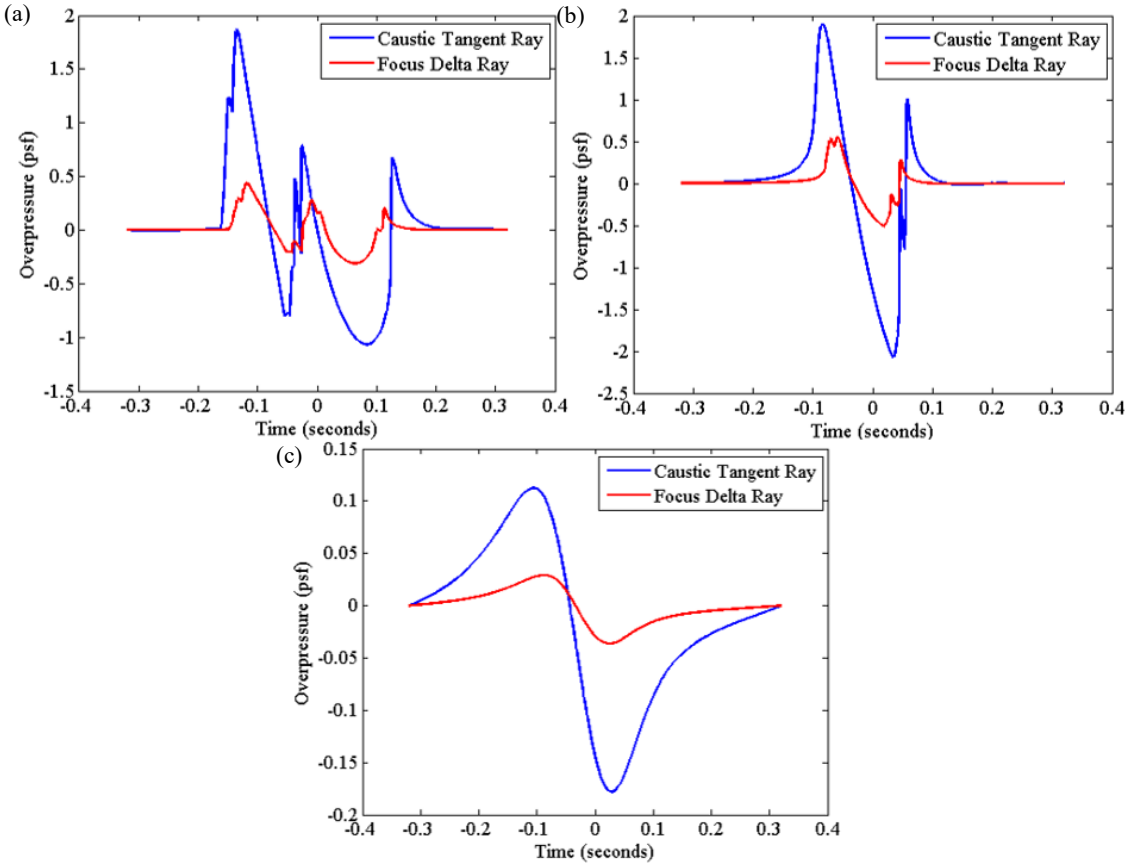

Figure 21. Ray comparison at $\bar{z}$ = (a) 1, (b) 0, and (c) −1

D. Refinement of method in January – March: hydrostatic atmospheric profile

The standard atmospheric profile provided for the focus case contained eight temperature points and pressure levels corresponding to standard atmospheric layers. Of those eight points, only two described the atmospheric conditions from the ground to the cruise altitude of 45,000 ft. This required FOBoom to interpolate a full set of temperature and pressure data in order to properly trace the ray and age the signature in PCBurg in 1,000 ft increments. Currently, FOBoom creates atmospheric profiles via linear interpolation. For improved accuracy, an atmospheric profile derived externally via the hydrostatic equations was substituted into FOBoom for the remainder of the analyses. Signatures computed with each atmospheric profile are compared in Figure 22**.** It is evident that the linear interpolated atmospheric profile predicts slightly higher peak overpressure, compared to the more accurate hydrostatic atmospheric profile. This phenomenon is consistent among all signatures calculated using LNTE at $\bar{z}$ = −1, 0, and 1. Future development of PCBoom detailed in Section VI could eliminate the need for an external hydrostatic interpolation process.

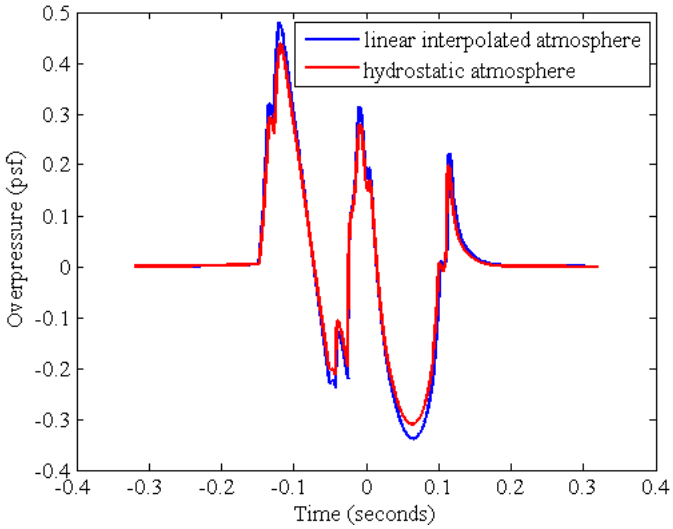

Figure 22. Atmospheric profile comparison at $\bar{z} = 1$

E. Refinement of method in January – March: $\bar{z}$ computation

Equation 3 represents the physical relationship to the dimensionless $\bar{z}$. This relationship is dependent on the characteristic acoustic frequency, the caustic curvature, and the diffraction boundary-layer thickness. The former is computed in LNTE from the PCBurg output file, whereas the latter two are calculated in FOBoom. A discrepancy was identified between the two computations because the characteristic acoustic frequency calculated by LNTE of approximately 13 Hz does not correspond to the resulting value of approximately 8 Hz according to the other two variable parameters in eq. 3. Therefore, the $\bar{z}$ locations reported by LNTE do not correspond to the true $\bar{z}$ locations. To reconcile this incongruence, signatures were extracted at corrected $\bar{z}$ values which correspond to the true target locations of −1, 0, and 1, based on the caustic curvature and diffraction boundary-layer thickness calculated in FOBoom. Further investigation of the LNTE code methodology will be required to discern the root of the characteristic acoustic frequency computational inconsistency.

The $\bar{z}$ = "1" signature calculated by LNTE predicts slightly higher peak overpressure due to its true location being closer to the ground at approximately $\bar{z} = 0.896$. As mentioned in section V.C, ground signatures and loudness metrics increase near the ground due to the significantly larger Blokhintsev parameter values at low altitudes. Figure 23 illustrates the signature at the true $\bar{z} = 1$ location in red as elongated in length, in addition to exhibiting slightly lower peak overpressure compared to the signature at $\bar{z} = 0.896$.

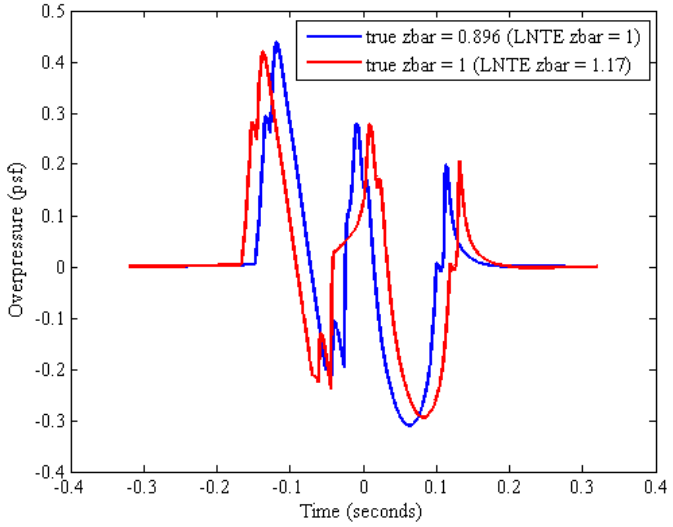

Figure 23. $\bar{z} = 1$ comparison

F. Final March revision results

Figure 24 displays the pressure vs. time signatures at each of the three specified $\overline{z}$ locations: 1, 0, and −1, as well as two additional locations at $\overline{z}$ = −3 and −7. SBPW3 organizers requested that the revised submission include the additional signatures which extend further into the shadow zone behind the caustic, in order to compare results between differing caustic-handling computational algorithms.

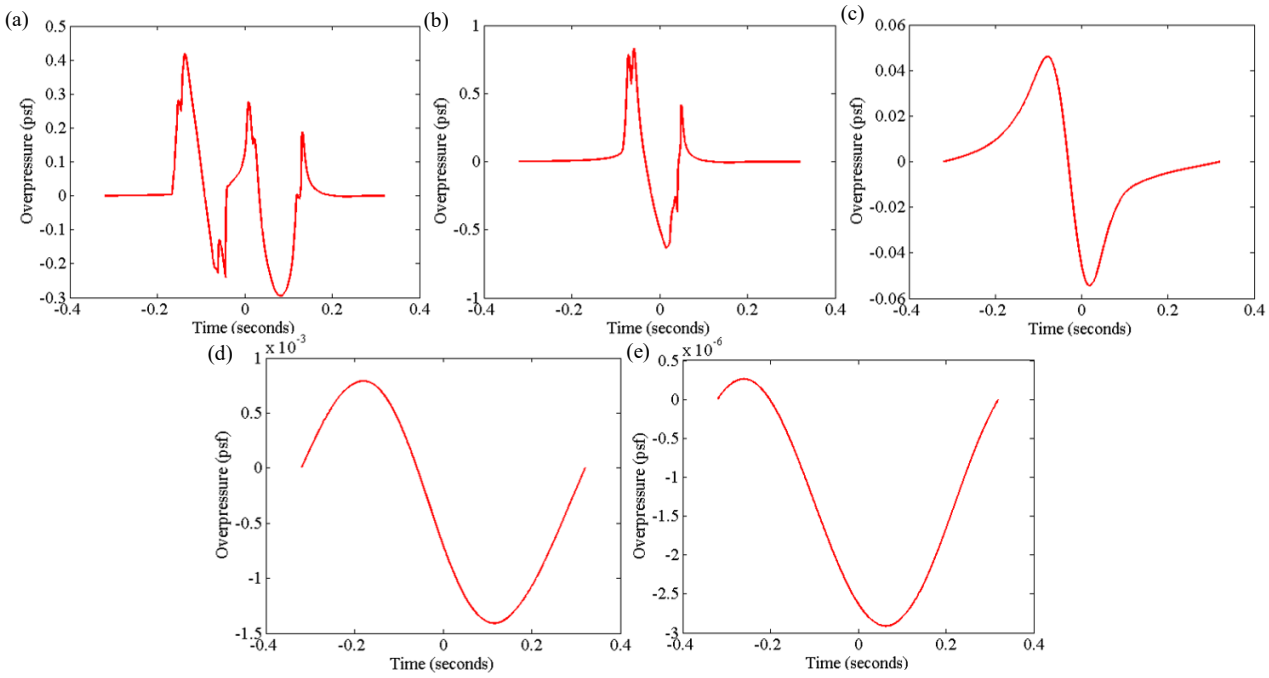

Figure 24. March final submittal signature at $\overline{z}$ = (a) 1, (b) 0, (c) −1, (d) −3, and (e) −7

The general shape of each signature matches the expected results depicted in Figure 4**.** The outgoing waveform in the illuminated zone at true $\overline{z}$ = 1 in Figure 24(a) exhibits the coalescence of both the N and U-shaped waveforms. The waveform closest to the caustic location at true $\overline{z}$ = 0 in Figure 24(b) includes only the single U-shaped waveform. The waveforms behind the caustic in the shadow zone at true $\overline{z}$ = −1, −3, and −7 in the shadow zone displayed in Figure 24(c) – (e) demonstrate heavily attenuated waveforms with rounded shocks and very low peak overpressures. Note that the peak overpressure calculated at the negative $\overline{z}$ locations decreases by several orders of magnitude as the distance from the caustic increases.

Table 4 displays the loudness metrics for all five of the above signatures. As expected, the signature at $\overline{z}$ = 0 exhibited the highest loudness metrics across the board, and the negative $\overline{z}$ signatures exhibit extremely low loudness metrics which decrease as displacement from the caustic increases. The 0 PLdB values computed from the negative $\overline{z}$ signatures suggest that the sound may be imperceptible at those locations. Note that the metrics were computed in LCASB which does not currently include the BSEL computation algorithm.

Table 4. March submittal loudness metrics in dB by $\overline{z}$

$\overline{z}$	PL	ASEL	CSEL
$\overline{z}$ = 1	86.11	71.88	93.62
$\overline{z}$ = 0	91.09	76.27	98.89
$\overline{z}$ = −1	0.00	3.30	64.99
$\overline{z}$ = −3	0.00	−5.18	22.02
$\overline{z}$ = −7	0.00	−24.96	−13.49

Table 5 displays the ground intersection data for the signature at $\overline{z}$ = 0. The *x* value represents distance along the ground plane from the aircraft, and the *z* value represents the ground height. The *y* value is zero because the aircraft heading is aligned with the positive *x* direction and there were no winds in the focus case. The *t* value represents propagation time from the aircraft to the ground.

Table 5. March submittal ground intersection data at $\bar{z} = 0$

x (ft)	y (ft)	z (ft)	t (seconds)
53,196.9	0	190.28	60.698

VI. Conclusion

As a result of modeling the SBPW3 cases using the PCBoom suite of tools, best practices were refined. A summary of lessons learned as a result of this work includes:

- The FOBoom automatic lateral cutoff angle algorithm results in angles smaller than those found using manually specified azimuths. In the latter scenario, results must be evaluated critically.
- For application of legacy FOBoom versions in scenarios where array limits are restrictive, the Ramer-Douglas-Peucker algorithm is a robust method of downsampling input data, though some user input and iteration are needed to determine appropriate tolerances. FOBoom Version 7 does not have the same restrictions.
- For PCBurg / HeadlessBurgers lossy propagation modeling, higher sampling rates tend to show better converged results in terms of metric levels. Although the time-step factor can be reduced to improve numerical stability, doing so can also introduce numerical noise in some scenarios; this is evident in ambient sections of pressure signatures.

This analysis identified several potential modifications to the PCBoom suite of tools that can improve the efficiency and accuracy of PCBoom analyses. These include:

- Add a hydrostatic mode keyword in FOBoom to internally calculate an accurately interpolated atmospheric profile
- Adapt HeadlessBurgers to create LNTE inputs
- Add the capability to PCBurg to output signatures at user-specified altitude(s), including via the command line capability to output signatures at user-specified altitude(s) would also be useful as a general analysis option.
- Streamlining the PCBoom process to automatically handle the appropriate LNTE interface geometry
- Investigating the characteristic acoustic frequency computation algorithms across PCBoom modules

Based on capability gaps and topics which may be relevant in coming years, some suggestions for the next Sonic Boom Prediction Workshop include:

- Inclusion of atmospheric turbulence effects on waveform signatures and metrics
- Additional focus cases: centerline and lateral positions. (Lateral cases might require a 3D Tricomi solver or possibly some sort of coordinate transformation/reference geometry)
- Investigation of the effects of vertical wind speeds on boom propagation and lateral cutoff locations
- Over-the-top propagation signature and metrics
- Prediction of signatures and metrics received by elevated microphones
- Prediction of booms over varying terrain

Appendix

Metrics calculated from ground signatures in each of the propagation cases are tabulated in this appendix. Extreme azimuth angles in each table represent rays at lateral cutoff locations.

Table 6. Case 1 ground metrics, modeled using FOBoom 7.0.1 with full resolution starting signatures and HeadlessBurgers with sampling rate 102.4 kHz

Azimuth angle	PL	ASEL	BSEL	CSEL
−78.3	39.3	35.55	55.81	71.63
−70	64.0	51.77	69.43	82.85
−60	69.8	55.90	73.01	86.30
−50	72.9	58.56	74.64	88.15
−40	74.5	60.61	75.74	89.47
−30	76.1	62.17	76.61	90.19
−20	74.9	60.05	76.38	90.75
−10	75.7	61.16	76.90	91.06
0	75.5	61.36	76.60	90.99
10	75.6	61.05	76.81	90.98
20	74.6	59.83	76.20	90.60
30	75.7	61.82	76.34	89.98
40	73.9	60.07	75.35	89.18
50	71.9	57.69	74.07	87.74
60	67.8	54.35	71.95	85.50
69.0	47.2	39.87	58.78	73.39

Table 7. Case 2 ground metrics, modeled using FOBoom 7.0.1 with full resolution starting signatures and HeadlessBurgers with sampling rate 102.4 kHz

Azimuth angle	PL	ASEL	BSEL	CSEL
−63.9	41.8	34.70	52.04	66.54
−62	63.5	51.12	65.40	77.30
−60	68.1	55.23	68.84	80.23
−50	74.8	61.39	74.54	85.35
−40	76.1	62.25	75.14	86.73
−30	77.1	63.79	75.73	87.65
−20	76.3	62.52	75.14	88.33
−10	75.8	62.2	74.89	88.90
0	75.9	62.38	75.04	89.16
10	76.0	62.35	75.03	89.02
20	76.6	62.85	75.44	88.59
30	77.6	64.33	76.22	88.10
40	77.1	63.19	75.97	87.48
50	76.5	62.90	76.04	86.79
60	74.6	61.43	74.05	84.64
62	73.6	60.34	73.20	83.93
64	72.2	59.10	72.20	83.10
66	70.8	57.60	70.96	82.07
68	68.6	55.53	69.25	80.67
70	63.6	51.30	65.62	77.53
70.5	57.0	45.52	60.54	72.99

Table 8. Case 2 standard atmosphere ground metrics, modeled using FOBoom 7.0.1 with full resolution starting signatures and HeadlessBurgers with sampling rate 102.4 kHz

Azimuth angle	PL	ASEL	BSEL	CSEL
−44.8	75.5	61.30	76.72	89.17
44.8	75.5	61.30	76.72	89.17

Acknowledgments

This work was funded by The U.S. Federal Aviation Administration under project number FB48CS00 and by the National Aeronautics and Space Administration under project number VXAHA119.

References

[1] Park, M. A., and Morgenstern, J. M., "Summary and Statistical Analysis of the First AIAA Sonic Boom Prediction Workshop," *Journal of Aircraft*, Vol. 53, No. 2, 2016, pp. 578–598. doi: 10.2514/1.C033449

[2] Rallabhandi, S. K. and Loubeau, A., "Summary of Propagation Cases of the Second AIAA Sonic Boom Prediction Workshop," *Journal of Aircraft*, Vol. 56, No. 3, 2018, pp. 876–895. doi: 10.2514/1.C034805

[3] Page, J. A., Plotkin, K. J., and Wilmer, C., "PCBoom Version 6.6 Technical Reference and User Manual," Wyle Report 10-10, December 2010.

[4] Thomas, C. L., "Extrapolation of Sonic Boom Pressure Signatures by the Waveform Parameter Method," NASA TN D-6832, June 1972.

[5] Plotkin, K. J., and Cantril, J. M., "Prediction of Sonic Boom at a Focus," Wyle Laboratories Research Report WR 75-7, October 1975. Also, AIAA Paper 76-2, January 1976. doi: 10.2514/6.1976-2

[6] Middleton, W.D., and Carlson, H. W., "A Numerical Method for Calculating Near-Field Sonic-Boom Pressure Signatures," NASA TN D-3082, November 1965.

[7] Plotkin, K. J., Page, J. A., and Haering, E. A., "Extension of PCBoom to Over-The-Top Booms, Ellipsoidal Earth, and Full 3-D Ray Tracing," AIAA Paper 2007-3677, May 2007. doi: 10.2514/6.2007-3677

[8] Crow, S. C., "Distortion of Sonic Bangs by Atmospheric Turbulence," *Journal of Fluid Mechanics*, Vol. 37, No. 3, 1969, pp. 529–563. doi: 10.1017/S0022112069000711

[9] Locey, L. L., Sparrow, V. W., and Piacsek, A. A., "Sonic Boom Post Processing to Include Atmospheric Turbulent Effects," AIAA Paper 2008-3035, May 2008. doi: 10.2514/6.2008-3035

[10] Stout, T. A., "Simulation of N-Wave and Shaped Supersonic Signature Turbulent Variations," Ph.D. Dissertation, Acoustics Dept., Pennsylvania State Univ., State College, PA, 2018.

[11] Page, J. A., Plotkin, K. J., Hobbs, C., Sparrow, V. W., Salamone, J., Cowart, R., Welge, H. R., Ladd, J., Maglieri, D., and Piacsek, A., "Superboom Caustic Analysis and Measurement Program (SCAMP) Final Report," NASA/CR–2015–218871, August 2015.

[12] Salamone, J. A., "Solution of the Lossy Nonlinear Tricomi Equation With Application to Sonic Boom Focusing," Ph.D. Dissertation, Acoustics Dept., Pennsylvania State Univ., State College, PA, 2013.

[13] Stevens, S. S., "Perceived Level of Noise by Mark VII and Decibels (E)," *Journal of the Acoustical Society of America*, Vol. 51, No. 2, part 2, 1972, pp. 575–601. doi: 10.1121/1.1912880

[14] Lonzaga, J. B., "Recent Enhancements to NASA's PCBoom Sonic Boom Propagation Code," AIAA Paper 2019-3386, June 2019. doi: 10.2514/6.2019-3386

[15] Ramer, U., "An Iterative Procedure for the Polygonal Approximation of Plane Curves," *Computer Graphics and Image Processing*, Vol 1, No. 3, 1972, pp. 244–256. doi: 10.1016/S0146-664X(72)80017-0

[16] Bolander, C. R., Hunsaker, D. F., Shen, H., and Carpenter, F. L., "Procedure for the Calculation of the Perceived Loudness of Sonic Booms," AIAA Paper 2019-2091, January 2019. doi: 10.2514/6.2019-2091

[17] LCASB, Loudness Code for Asymmetric Sonic Booms, Software Package, Ver. 1.0.0.1, NASA Langley Research Center, Hampton, VA, Reference Number LAR-16954-1.

[18] Salamone, J. A., Sparrow, V. W., Plotkin, K. J., and Cowart, R., "SCAMP: Solution of the Lossy Nonlinear Tricomi Equation for Sonic Boom Focusing," AIAA Paper 2013-0935, January 2013. doi: 10.2514/1.J052171

[19] Auger, T., and Coulouvrat, F. "Numerical Simulation of Sonic Boom Focusing," *AIAA Journal,* Vol 40, No. 9, 2002, pp. 1726–1734. doi: 10.2514/2.1877

[20] Rallabhandi, S. K., "Propagation Analysis of the 3rd Sonic Boom Prediction Workshop Cases using sBOOM", AIAA SciTech, January 2021 (to be submitted for publication)